COMPUTING AND ALGORITHM INSIGHT
Volume 4, Issue 1, June 2026 | pp. 75-88
https://doi.org/10.63208/21018-243

OPEN ACCESS
Check for updates

ENHANCING EFFICIENCY AND TRANSPARENCY IN DISEASE DIAGNOSIS VIA RANDOMIZED MACHINE LEARNING AND EXPLAINABLE AI

Wu Zeyu[1] ✉, Tang Lijuan[1], and Liang Hao[2]

School of Artificial Intelligence, Beijing University of Technology, Beijing, China[1]; School of Computer and Software, Nanjing University of Information Science and Technology, Nanjing, China[2]

ABSTRACT

Deep learning has significantly advanced medical diagnostics through big data utilization; however, high computational costs and "black-box" opacity remain critical barriers in resource-constrained clinical settings. This research investigates randomized machine learning frameworks specifically Extreme Learning Machines (ELMs) and Random Vector Functional Link (RVFL) networks as efficient alternatives. By incorporating stochasticity into the training phase, these architectures reduce computational complexity and latency without compromising diagnostic precision. To mitigate interpretability concerns, the study integrates Explainable AI (XAI) tools, including Local Interpretable Model-agnostic Explanations (LIME) and Shapley Additive Explanations (SHAP), to elucidate model decision-making. Empirical evaluations involving genitourinary cancers and coronary artery disease datasets reveal that RVFL superiorly balances performance and efficiency, achieving accuracies of 88.29% and 81.64% with significantly reduced processing times (6.22s and 0.0308s, respectively). These findings advocate for the adoption of randomized models to enhance transparency and operational speed in healthcare, ultimately facilitating more accessible, interpretable, and timely diagnostic interventions.

Keywords: *Randomized Machine Learning, Extreme Learning Machines, Explainable AI, Medical Diagnostics, Computational Efficiency.*

CORRESPONDING AUTHOR:
Wu Zeyu
School of Artificial Intelligence, Beijing University of Technology, Beijing, China
contact: *wuzeyu@bjut.edu.cn*

ARTICLE HISTORY
Received : January 7, 2026
Final Revised : May 18, 2026
Accepted : June 10, 2026
Published : June 30, 2026

© 2026 The Author(s) | Published by Integra Academic Press | This article is an open access article and distributed under the terms and conditions of the Creative Commons Attribution (CC BY-SA) license.

1. | INTRODUCTION

Deep learning (DL) architectures have revolutionized healthcare by facilitating high-precision disease diagnosis and clinical data interpretation through the analysis of massive datasets [1]. However, the reliance on back-propagation algorithms and extensive weight updates results in significant time complexity and high computational demands [2]. As these models grow in depth, the associated increase in execution time creates a critical bottleneck in time-sensitive and resource-constrained medical scenarios [3], [4]. Furthermore, the "black-box" nature of DL systems obscures the rationale behind clinical decisions [5], conflicting with regulatory frameworks like the GDPR, which mandate transparency in automated decision-making [6]. Additionally, the substantial energy consumption and carbon footprint of large-scale data centers raise urgent sustainability concerns, necessitating the development of greener AI practices [7].

To mitigate these challenges, randomization-based algorithms offer a promising alternative by introducing stochasticity into the training process, thereby reducing computational complexity and latency while maintaining accuracy [8]. This paper proposes an explainable AI framework utilizing Extreme Learning Machines (ELMs) [9] and Random Vector Functional Link (RVFL) networks [10]. We evaluate these models against benchmark neural and recurrent architectures using two case studies: genitourinary cancer and coronary artery disease prediction. By integrating Local Interpretable Model-agnostic Explanations (LIME) and Shapley Additive Explanations (SHAP), we address the lack of transparency in randomized models, enhancing clinical trust.

2. | LITERATURE REVIEW

Ravi et al. [11] provided a comprehensive evaluation of deep learning in health informatics, noting that while DNNs offer significant potential, they are hindered by extensive training periods and high computational requirements. Similarly, Lundervold and Lundervold [12] identified interpretability as a primary limitation in medical imaging, where the "black-box" nature of hierarchical representations obscures the logic behind predictions. Yu et al. [13] further corroborated these findings by highlighting systemic challenges in genomics and medical imaging, specifically regarding integration, scalability, and the substantial power needed for automation.

Beyond computational hurdles, Bansal et al. [14] emphasized that the necessity for massive datasets to prevent overfitting poses a significant barrier in data-scarce domains like medical science, especially where privacy concerns limit accessibility. Hossain et al. [15] noted that while deep learning excels at feature extraction, its complexity impedes deployment on resource-constrained IoT and wearable devices, fueling a constant search for faster, more efficient algorithms [16]. This sentiment is echoed by Baskakov and Arseniev [17], who identified the reduction of DNN complexity as a vital frontier for both theoretical advancement and hardware development.

The prevailing literature [18] underscores an urgent need for computationally lean techniques. Current attempts to simplify architectures often result in performance trade-offs; thus, there is a pressing requirement for innovative frameworks that balance efficiency with efficacy. Such novel architectures must provide high-level performance without the prohibitive training times of traditional DNNs, while simultaneously enhancing model explainability.

3. | METHODOLOGY

3.1 Datasets

Our research utilizes two distinct clinical datasets for model validation:

- Genitourinary Cancers: This dataset involves 1,337 patients from Mackay Memorial Hospital (2017–2021), featuring 39 physiological and lifestyle variables. The predictors encompass diverse biochemical markers—including renal and liver function indicators like Albumin, Creatinine, and AST/ALT—alongside exhaustive urinalysis measures such as Nitrite, pH, and Protein levels. To ensure clinical depth, demographic and behavioral factors (e.g., age, smoking, and family history) were integrated. The dataset covers malignancies including kidney, prostate, bladder, cystitis, and uterine cancers, with all diagnoses validated by consultants and pathology reports.
- Coronary Artery Disease: Sourced from the UCI Machine Learning repository [19], this dataset consists of 303 patient records with 13 key features. It serves as a benchmark for evaluating diagnostic models in the context of cardiovascular health.

The selection of these datasets provides a multifaceted basis for testing the model's accuracy across varied physiological parameters and disease types.

3.2 Data Pre-Processing

To maintain dataset quality and ensure algorithmic compatibility, a multi-stage preprocessing workflow was implemented. Missing values were initially imputed using the column mean to preserve data integrity. The datasets were then partitioned into feature set X and target variable Y, with categorical labels converted into numerical representations via one-hot encoding [20]. Subsequently, the data was stratified into training (70%) and testing (30%) subsets to facilitate robust model evaluation [21]. Finally, a "StandardScaler" was applied to normalize the feature space, ensuring each variable contributes uniformly by centering the distribution to a mean of zero and a standard deviation of one [22].

3.3 Randomization-Based Learning Models

The proposed framework utilizes two randomization-based architectures, beginning with Extreme Learning Machines (ELMs). ELMs are single-hidden layer feedforward networks optimized for rapid training and high-performance efficiency [23]. Unlike conventional backpropagation methods, ELMs employ a fixed, stochastic initialization for the input weights and hidden layer biases. Consequently, the training phase is simplified to a linear optimization of the weights connecting the hidden layer to the output layer, significantly decreasing computational complexity. For an input matrix $X \in R^{N\times d}$ and a target matrix $Y \in R^{N\times m}$, the hidden layer transformation is mathematically defined as:$H = g(XW + b)$, where $W \in R^{d\times L}$ and $b \in R^{\mathbb{1}\times L}$ represent the randomly generated, static weight matrix and bias vector for L hidden nodes, respectively, and $g(\cdot)$ is the activation function. The model's final output is derived as $O = H\beta$, where β denotes the output weight matrix. The optimization goal is to minimize the discrepancy between the predicted output O and the actual target Y, typically resolved as a least-squares problem in (1):

$$\min_{\beta} |H\beta - Y|^2 + \lambda|\beta|^2 \quad (1)$$

To mitigate the risk of overfitting, a regularization parameter λ is incorporated into the objective function. The resulting optimization problem, presented in (1), is solved analytically using the closed-form expression shown in (2):

$$\beta = (H^T H + \lambda I)^{-1} H^T Y \tag{2}$$

The architectural configuration of the ELMs in this research utilizes a single input layer, a variable number of hidden layers ranging from one to four (selected stochastically) equipped with ReLU activation, and a final output layer employing a SoftMax function. To ensure robust generalization and prevent the model from learning irrelevant noise within the training set, L2 regularization was implemented as a primary strategy to mitigate overfitting.

The Random Vector Functional Link (RVFL) network improves learning efficiency by augmenting standard hidden layers with direct connections between input and output layers [24]. Similar to ELMs, the internal weights remain stochastic and static, restricting training to the optimization of output weights. This architectural modification significantly reduces computational overhead. Mathematically, the output $O \in R^{N\times m}$ integrates contributions from the hidden layer H and the direct input links X:$O = HW_{hidden} + XW_{input}$ where $W_{hidden} \in R^{L\times m}$ and $W_{input} \in R^{d\times m}$ denote the respective weight matrices. To determine the optimal weights while minimizing loss against the target Y, Tikhonov regularization [25] is employed as follows in (3):

$$W^* = \arg\min_W |HW_{hidden} + XW_{input} - Y|^2 + \lambda |W|^2 \tag{3}$$

In this formulation, λ serves as the regularization parameter to ensure numerical stability and generalization. The optimal weight matrices for the direct and hidden connections, W^*_{input} and W^*_{hidden}, are derived analytically through the following closed-form expressions in (4) and (5):

$$W^*_{input} = (X^\top X + \lambda I)^{-1} X^\top Y \tag{4}$$

$$W^*_{hidden} = (H^\top H + \lambda I)^{-1} H^\top Y \tag{5}$$

Our RVFL implementation utilizes stochastically initialized hidden layer weights and biases, with node activations processed via the $tanh$ function. To enhance the feature space, polynomial expansion of degree 2 is applied to the hidden layer outputs. Furthermore, the output weights are optimized by tuning the regularization parameter, effectively balancing non-linear transformations and polynomial features to maximize predictive performance without compromising computational efficiency.

3.4 Benchmark Models

To establish a comparative baseline, we utilized the following benchmark architectures:

- Deep Neural Network (DNN): Characterized by multiple hierarchical layers, the DNN facilitates the extraction of complex patterns through non-linear transformations [26]. Our implementation features an input layer, four hidden layers with varying node densities utilizing ReLU activation, and a SoftMax output layer. Loss functions were tailored to the specific diagnostic task: binary cross-entropy for coronary artery disease and categorical cross-entropy for multi-class genitourinary cancer classification.

- Recurrent Neural Network (RNN): This model incorporates a Simple RNN layer to capture temporal or sequential dependencies within the training data dimensions [27]. This is succeeded by three fully connected hidden layers using ReLU activation. The final Dense output layer employs a SoftMax function to generate the probability distributions necessary for diagnosis.
- Simple Neural Network (SNN): A foundational architecture comprising an input layer, a single hidden layer with ReLU activation, and an output layer [28]. The output stage utilizes SoftMax for the genitourinary dataset and a Sigmoid function for binary heart disease classification, enabling basic non-linear mapping with minimal computational complexity.

3.5 Explainable Artificial Intelligence (XAI)

To enhance the transparency of the proposed framework, we integrate Explainable AI (XAI) techniques, specifically LIME and SHAP, to bridge the gap between complex algorithmic outputs and human interpretability.

- LIME: Local Interpretable Model-agnostic Explanations (LIME) provide a methodology for generating comprehensible insights into individual predictive outcomes [29]. This approach simplifies complex decision boundaries by constructing a locally faithful, interpretable approximation of the model's behavior around a specific data point. The mathematical formulation for this local surrogate approach is expressed in (6).

$$L(f, g, \pi_x) + \Omega(g) = \sum_{i=1}^{N} w_i \cdot \left(f(x_i') - g(x_i')\right)^2 + \Omega(g) \quad (6)$$

The local surrogate model g is designed to approximate the original model's prediction f within the proximity of x. This approach utilizes weights w_i, calculated via the proximity measure π_x, to evaluate perturbed instances x_i' based on a distance metric $d(x, x_i')$ and kernel width σ. As shown in (6), the objective function combines a fidelity term $L(f, g, \pi_x)$ to ensure g accurately reflects f locally, with a complexity term $\Omega(g)$ to maintain interpretability. The training of g over N perturbations ensures the local faithfulness and explanatory power of the LIME framework.

- SHAP: Derived from cooperative game theory, SHapley Additive exPlanations (SHAP) demystifies machine learning predictions by quantifying the contribution of each feature to a specific outcome [30]. By treating each prediction as a strategic game, SHAP assigns an importance score the Shapley value (ϕ_i) to each feature i, ensuring an equitable distribution of the model's output among its predictors. The fundamental mathematical calculation for these values is presented in (7).

$$\phi_i(v) = \sum_{S \subseteq N \setminus \{i\}} \frac{|S|!(|N|-|S|-1)!}{|N|!} [v(S \cup \{i\}) - v(S)] \quad (7)$$

The Shapley value $\phi_i(v)$ quantifies the contribution of feature i by evaluating the marginal change in the model's outcome across all possible feature combinations. As defined in (7), the term $v(S \cup \{i\}) - v(S)$ calculates the difference in prediction when feature i is included versus when it is excluded from a subset S of the total feature set N. The weighting factor, utilizing the cardinalities of S and N, ensures a mathematically balanced assessment of the feature's unique impact across every possible coalitional arrangement.

3.6 Evaluation Metrics

The performance of the ELM, RVFL, and benchmark models was assessed using standard evaluation metrics, including accuracy, precision, recall, and the F1-score [31]. The classification results are detailed via the confusion matrix in Table 1, while the formal definitions for each performance metric are provided in Table 2.

Table 1. Confusion Matrix.

	Predicted True	**Predicted False**
Actual True	True Positive (TP)	False Negative (FN)
Actual False	False Positive (FP)	True Negative (TN)

Table 2. Performance Metrics.

Name	**Formula**
Accuracy	(TP+TN) / (TP+TN+FP+FN)
Recall	TP / (TP+FN)
Precision	TP / (TP+FP)
F1-Score	2 * (Precision * Recall) / (Precision + Recall)

4. | RESULTS AND DISCUSSION

This section evaluates the performance of the proposed framework relative to the benchmark algorithms across both case studies. The ELM, RVFL, and comparison models (SNN, RNN, and DNN) were implemented in Python on a system powered by an AMD Ryzen 7 5700X Eight-Core CPU and a 16 GB NVIDIA GEFORCE RTX 4080 GPU. The results for each case study are detailed in the following subsections.

4.1 Results Using Genitourinary Cancers Dataset

Table 4 summarizes the comparative performance of randomization-based and benchmark models for multi-class classification on the Genitourinary Cancers dataset. The DNN achieved an accuracy of 82.98%, with precision and recall at 82.91% and 82.98% respectively, yielding a balanced F1-score of 82.36% but requiring a substantial training time of 13.9 seconds. Despite its simpler architecture, the SNN marginally surpassed the DNN with 83.76% accuracy and an F1-score of 82.80%, though it exhibited a slight efficiency trade-off with a training duration of 14.25 seconds. The RNN, while obtaining a robust F1-score of 83.37% and 83.42% accuracy, incurred the highest computational overhead, necessitating 18.82 seconds to complete training.

Table 3. Performance evaluation of ELM, RVFL, and benchmark models for Genitourinary Cancer prediction.

Approach	**Accuracy**	**Precision**	**Recall**	**F1-score**	**Training Time in Second**
DNN	82.98	82.91	82.98	82.36	13.9
SNN	83.76	83.94	83.76	82.80	14.25
RNN	83.42	83.34	83.42	83.37	18.82
ELMs	87.26	87.12	87.16	86.46	5.31
RVFL	88.29	88.43	88.29	87.38	6.22

The ELM model significantly improved performance, achieving an accuracy of 87.26%, precision of 87.12%, and a recall of 87.16%, supported by a robust F1-score of 86.46%. Its exceptional efficiency was highlighted by a minimal training duration of only 5.31 seconds. However, the RVFL emerged as the optimal architecture, securing the highest accuracy of

88.29%, along with a precision of 88.43% and a matching recall. The superior predictive strength of the RVFL is further evidenced by an F1-score of 87.38% and its robust AUC-ROC curve in Fig. 1. With a training time of 6.22 seconds, the RVFL effectively balanced high diagnostic precision with computational efficiency, making it the most effective approach in this study.

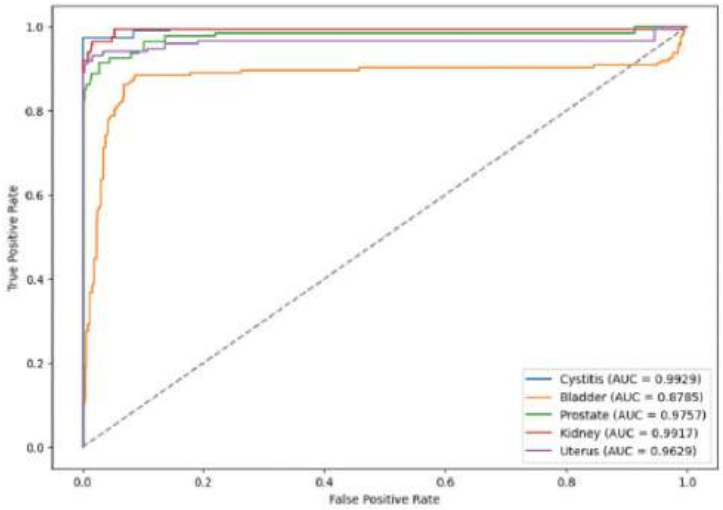

Figure 1. ROC curves for classification of genitourinary cancers.

The feature contributions for genitourinary cancer prediction are visualized through LIME explanations in Fig. 2, where specific weights indicate their directional influence on the model's output. Variables such as Beetle Nut consumption, Urine Epithelium, Gender, Nitrate, Diabetes, and Glucose AC exhibit positive correlations, strongly driving the prediction toward a kidney cancer diagnosis. Conversely, Family History, Urine Glucose, and Protein levels contribute toward a "no cancer" classification. Furthermore, Fig. 3 illustrates that the synergistic effects of Glucose AC, Sodium, Beetle Nut, Urine Epithelium, Urine Ketone, and Estimated GFR significantly elevate the probability of kidney cancer, effectively overriding the negative contribution of Specific Gravity.

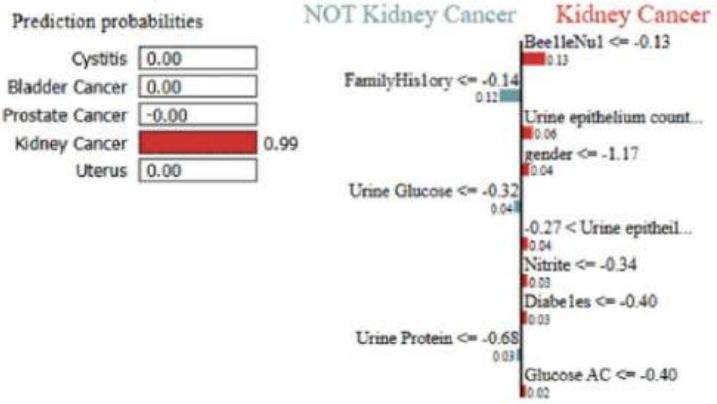

Figure 2. LIME explanations for kidney cancer.

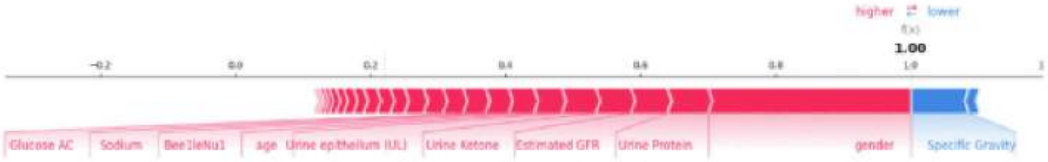

Figure 3. SHAP visualization for kidney cancer.

Fig. 4 illustrates the diagnostic explanations for Cystitis, where specific feature weights identify critical clinical indicators. The presence of Nitrites, a typical marker of bacterial infection, serves as a primary positive predictor for Cystitis. Additionally, lower Albumin levels, alcohol consumption, and Cholesterol, alongside urinalysis markers such as Glucose, Ketone, and Bilirubin, contribute quantifiably to this classification. In contrast, variables including Total Protein and the A/G Ratio are assigned weights that align with the absence of Cystitis, indicating that their observed thresholds do not satisfy the diagnostic criteria for the condition.

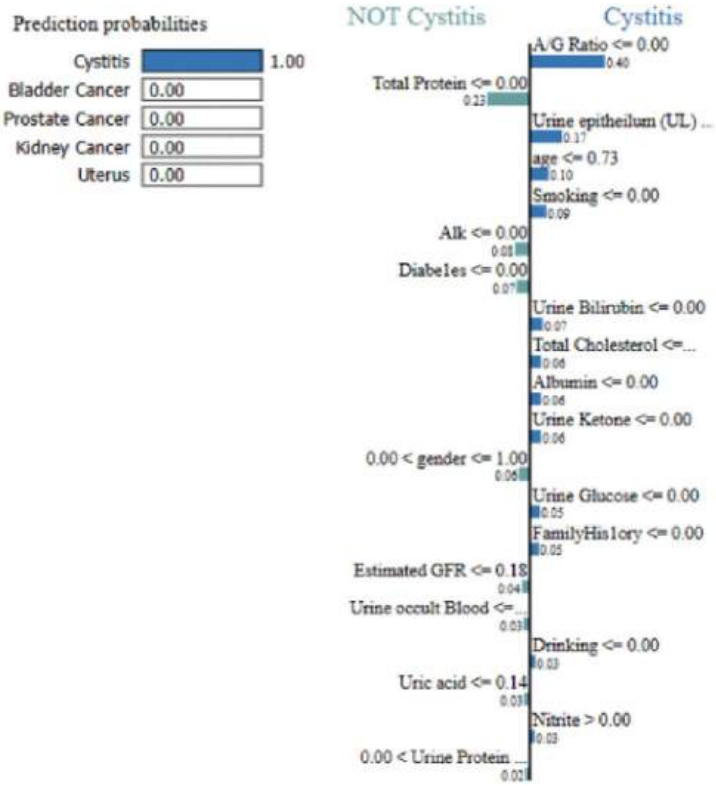

Figure 4. LIME explanations for cystitis.

As illustrated in Fig. 5, the collective influence of Albumin, ALK, A/G Ratio, and ALT (GPT) significantly increases the predicted probability of Cystitis, effectively counteracting the negative marginal contribution of AST (GOT). While SHAP explanations elucidate the primary laboratory features driving the model's output, they may not capture the exhaustive range of biomarkers that could potentially exert substantial positive or negative impacts on the final diagnostic decision.



Figure 5. SHAP visualization for cystitis.

4.2 Coronary Artery Disease Dataset

Table 4 provides a comparative analysis of the evaluation metrics and computational efficiency for all investigated models.

Table 4. Performance evaluation of ELM, RVFL, and benchmark models for Coronary Artery Disease prediction.

Approach	Accuracy	Precision	Recall	F1-score	Training Time (s)
DNN	75.82	76.23	75.82	75.88	6.65
SNN	73.63	73.68	73.63	73.62	4.15
RNN	73.63	74.38	73.63	73.69	7.86
ELMs	76.45	76.24	76.15	76.15	0.021
RVFL	81.64	82.23	81.64	81.61	0.0308

According to Table 4, the DNN yielded an accuracy of 75.82% and an F1-score of 75.88, requiring 6.65 seconds for training. The SNN achieved lower metrics (73.63% accuracy; 73.62 F1-score) in 4.15 seconds, while the RNN matched the SNN's accuracy but incurred the highest training latency at 7.86 seconds. In contrast, the ELM significantly improved both performance and efficiency, securing a 76.45% accuracy within a remarkable 0.021 seconds. The RVFL emerged as the most effective model, reaching a peak accuracy of 81.64% and an F1-score of 81.61%. As illustrated by the AUC-ROC curve in Fig. 6, the RVFL's superior classification power is achieved with a minimal training duration of only 0.0308 seconds, demonstrating its high operational efficiency.

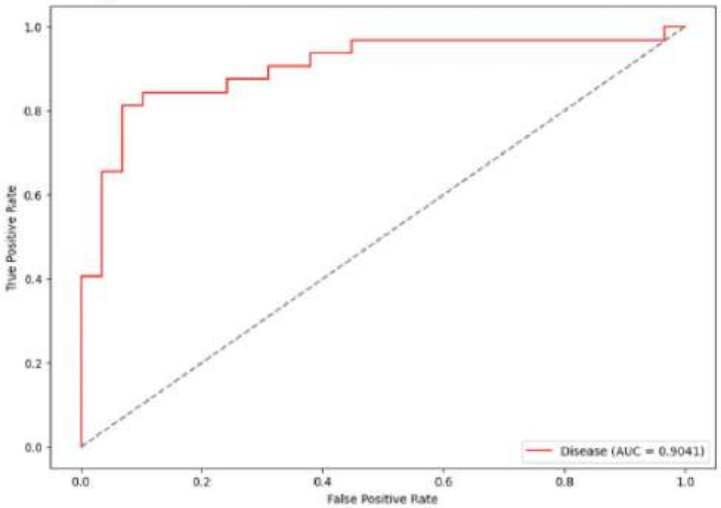

Figure 6. ROC curves for classification of coronary artery disease.

The feature contributions for coronary artery disease prediction are detailed via LIME in Fig. 7, where positive weights for features such as thal, exang, oldpeak, ca, cp, trestbps, and fbs indicate a strong influence toward a positive diagnosis. Conversely, slope, restecg, and age align with a "no disease" outcome. Furthermore, Fig. 8 utilizes SHAP values to quantify

individual feature impacts; variables including cp, slope, ca, oldpeak, fbs, and thalach drive the model toward a coronary artery disease prediction, whereas chol levels contribute negatively, favoring a healthy classification.

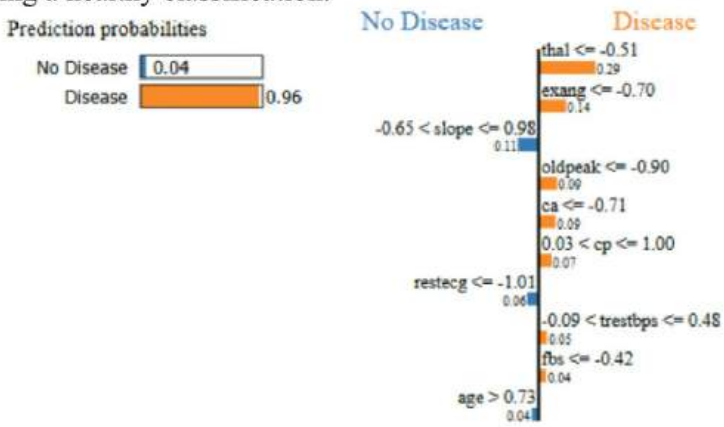

Figure 7. LIME explanations for coronary artery disease.

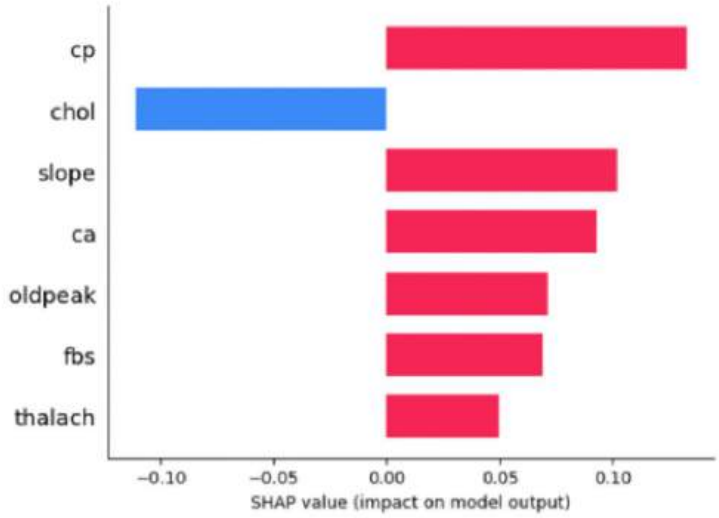

Figure 8. SHAP coronary artery disease.

4.2 Discussion

The performance gap between ELM, RVFL, and traditional architectures (DNN, SNN, RNN) in diagnosing Genitourinary Cancers and Coronary Artery Disease stems from fundamental differences in architecture and optimization. ELM and RVFL leverage stochastic initialization of input weights and biases, bypassing iterative training to significantly reduce computational overhead while maintaining high generalization capabilities. RVFL further enhances this by incorporating direct input-output links, allowing it to capture complex data relationships more robustly than the other models.

In contrast, while DNNs can model intricate patterns, their multi-layered depth necessitates extensive parameter optimization, leading to higher training times (e.g., 13.9s vs. 5.31s for ELM in the cancer dataset). SNNs, despite their relative simplicity, still rely on iterative processes that hinder efficiency. RNNs proved particularly inefficient for these static datasets; their specialized structure for temporal dependencies adds unnecessary computational burdens without providing significant accuracy gains.

Integrating XAI methods like LIME and SHAP with ELM and RVFL is pivotal for healthcare, as these techniques provide the transparency necessary for clinical trust—a feat more challenging to achieve with the inherent "black-box" complexity of deep architectures. Our findings align with existing literature, where ELMs are recognized for their fast, non-iterative learning [32], [33]. Furthermore, the efficacy of RVFL in managing non-linear medical data is well-documented, as seen in its successful application in complex diagnostic frameworks [34].

5. | CONCLUSION

This research addresses the computational inefficiencies of traditional DL architectures, such as DNN, RNN, and SNN, by proposing randomization-based alternatives, specifically ELM and RVFL. By leveraging stochastic training, these models minimize complexity and training latency while maintaining high predictive accuracy across two case studies: genitourinary cancer and coronary artery disease. Results indicate that RVFL achieves superior performance with minimal training time, while ELM also demonstrates enhanced efficiency compared to conventional methods. The integration of XAI techniques, LIME and SHAP further ensures diagnostic transparency, fostering trust in clinical AI applications.

Future research should evaluate the generalizability of these models by extending their application to neurological, respiratory, and infectious diseases. Furthermore, exploring the synergy between randomization-based learning and advanced paradigms, such as reinforcement learning or generative adversarial networks, presents a promising direction for developing more versatile medical diagnostic systems.

REFERENCES

1. G. Litjens et al., "A survey on deep learning in medical image analysis," Med. Image Anal., vol. 42, pp. 60–88, 2017.
2. I. Goodfellow, Y. Bengio, and A. Courville, Deep Learning. Cambridge, MA, USA: MIT Press, 2016.
3. Y. LeCun, Y. Bengio, and G. Hinton, "Deep learning," Nature, vol. 521, no. 7553, pp. 436–444, 2015.
4. D. Muhammad and M. Bendechache, "Unveiling the black box: A systematic review of explainable artificial intelligence in medical image analysis," Comput. Struct. Biotechnol. J., vol. 24, pp. 542–560, 2024.
5. S. Roy, D. Pal, and T. Meena, "Explainable artificial intelligence to increase transparency for revolutionizing healthcare ecosystem and the road ahead," Netw. Model. Anal. Health Informat. Bioinf., vol. 13, no. 1, 2023, Art. no. 4.
6. M. Grochowski, A. Jablonowska, F. Lagioia, and G. Sartor, "Algorithmic transparency and explainability for EU consumer protection: Unwrapping the regulatory premises," Crit. Anal. Law, vol. 8, pp. 43–63, 2021.
7. E. Strubell, A. Ganesh, and A. McCallum, "Energy and policy considerations for modern deep learning research," in Proc. AAAI Conf. Artif. Intell., 2020, pp. 13693–13696.
8. L. Zhang and P. N. Suganthan, "A survey of randomized algorithms for training neural networks," Inf. Sci., vol. 364, pp. 146–155, 2016.

9. G. Huang, G.-B. Huang, S. Song, and K. You, "Trends in extreme learning machines: A review," Neural Netw., vol. 61, pp. 32–48, 2015.
10. A. K. Malik, R. Gao, M. Ganaie, M. Tanveer, and P. N. Suganthan, "Random vector functional link network: Recent developments, applications, and future directions," Appl. Soft Comput., vol. 143, 2023, Art. no. 110377.
11. D. Ravì et al., "Deep learning for health informatics," IEEE J. Biomed. Health Informat., vol. 21, no. 1, pp. 4–21, Jan. 2017.
12. A. S. Lundervold and A. Lundervold, "An overview of deep learning in medical imaging focusing on MRI," Zeitschrift für Medizinische Physik, vol. 29, no. 2, pp. 102–127, 2019.
13. N. Yu, Z. Yu, F. Gu, T. Li, X. Tian, and Y. Pan, "Deep learning in genomic and medical image data analysis: Challenges and approaches," J. Inf. Process. Syst., vol. 13, no. 2, pp. 204–214, 2017.
14. M. A. Bansal, D. R. Sharma, and D. M. Kathuria, "A systematic review on data scarcity problem in deep learning: Solution and applications," ACM Comput. Surv. (CSUR), vol. 54, no. 10s, pp. 1–29, 2022.
15. M. S. Im and V. R. Dasari, "Computational complexity reduction of deep neural networks," 2022, arXiv:2207.14620.
16. M. B. Hossain, N. Gong, and M. Shaban, "Computational complexity reduction techniques for deep neural networks: A survey," in Proc. 2023 IEEE Int. Conf. Artif. Intell. Blockchain Internet Things, 2023, pp. 1–6.
17. D. Baskakov and D. Arseniev, "On the computational complexity of deep learning algorithms," in Proc. Int. Sci. Conf. Telecommun. Comput. Control, 2021, pp. 343–356.
18. N. C. Thompson, K. Greenewald, K. Lee, and G. F. Manso, "The computational limits of deep learning," 2020, arXiv:2007.05558.
19. A. Janosi, W. Steinbrunn, M. Pfisterer, and R. Detrano, "Heart disease," UCI Mach. Learn. Repository, 1989. [Online]. Available: https://doi.org/10.24432/C52P4X
20. E. Jang, S. Gu, and B. Poole, "Categorical reparameterization with gumbel-softmax," 2016, arXiv:1611.01144.
21. D. Muhammad, I. Ahmad, M. I. Khalil, W. Khalil, and M. O. Ahmad, "A generalized deep learning approach to seismic activity prediction," Appl. Sci., vol. 13, no. 3, pp. 1–13, 2023.
22. M. M. Ahsan, M. A. P. Mahmud, P. K. Saha, K. D. Gupta, and Z. Siddique, "Effect of data scaling methods on machine learning algorithms and model performance," Technologies, vol. 9, no. 3, pp. 1–17, 2021.
23. G.-B. Huang, D. H. Wang, and Y. Lan, "Extreme learning machines: A survey," Int. J. Mach. Learn. Cybern., vol. 2, pp. 107–122, 2011.
24. L. Zhang and P. N. Suganthan, "A comprehensive evaluation of random vector functional link networks," Inf. Sci., vol. 367, pp. 1094–1105, 2016.
25. G. H. Golub, P. C. Hansen, and D. P. O'Leary, "Tikhonov regularization and total least squares," SIAM J. Matrix Anal. Appl., vol. 21, no. 1, pp. 185–194, 1999.
26. D. Muhammad, N. Rafiullah, and M. Bendechache, "Improving diagnostic trust: An explainable deep learning framework for genitourinary cancer prediction," IET Conf. Proc., vol. 2024, pp. 47–54, 2024.
27. S. Grossberg, "Recurrent neural networks," Scholarpedia, vol. 8, no. 2, pp. 1–21, 2013, doi: 10.4249/scholarpedia.1888.

28. E. Brown, J. Gao, P. Holmes, R. Bogacz, M. Gilzenrat, and J. D. Cohen, "Simple neural networks that optimize decisions," Int. J. Bifurcation Chaos, vol. 15, no. 03, pp. 803–826, 2005.
29. Y. Wu, M. N. Rabe, W. Li, J. Ba, R. B. Grosse, and C. Szegedy, "LIME: Learning inductive bias for primitives of mathematical reasoning," in Proc. Int. Conf. Mach. Learn., 2021, pp. 11251–11262.
30. G. Van den Broeck, A. Lykov, M. Schleich, and D. Suciu, "On the tractability of SHAP explanations," J. Artif. Intell. Res., vol. 74, pp. 851–886, 2022.
31. I. Ahmad, M. A. Alqarni, A. A. Almazroi, and A. Tariq, "Experimental evaluation of clickbait detection using machine learning models," Intell. Autom. Soft Comput., vol. 26, no. 6, pp. 1335–1344, 2020.
32. D. C. E. Saputra, K. Sunat, and T. Ratnaningsih, "A new artificial intelligence approach using extreme learning machine as the potentially effective model to predict and analyze the diagnosis of anemia," Healthcare, vol. 11, no. 5, pp. 1–25, 2023.
33. X. Liu, Y. Zhou, W. Meng, and Q. Luo, "Functional extreme learning machine for regression and classification," Math. Biosci. Eng., vol. 20, no. 2, pp. 3768–3792, 2023.
34. R. Sharma, T. Goel, M. Tanveer, P. Suganthan, I. Razzak, and R. Murugan, "Conv-eRVFL: Convolutional neural network based ensemble RVFL classifier for Alzheimer's disease diagnosis," IEEE J. Biomed. Health Informat., vol. 27, no. 10, pp. 4995–5003, Oct. 2023.